A reconfigurable multi-mode mobile parallel robot

A Reconfigurable Multi-mode Mobile Parallel Robot

Yaobin Tian, Dan Zhang*, Yan-An Yao*, Xianwen Kong, and Yezhuo Li

***Abstract*—**In this paper we put forward the idea of deforming the geometry of a parallel mechanism such that it can operate either as an equivalent rolling robot or quadruped robot. Based on it, we present a novel mobile parallel robot that can change its locomotion modes via different equivalent mechanisms. The robot is in essence a four-arm parallel mechanism in which each arm contains five revolute (R) joints. The axes of the three internal R joints in any arm are parallel and are orthogonal to those of the end joints. Based on singularity and deformation analysis, we show that the upper platform has four practical operation modes, (i.e., translation, planar, rotational, and locked-up modes). Using these operation modes, the robot can realize rolling, tumbling and quadruped locomotion modes by deforming into switching states. The switching configurations of the robot are further identified in which the robot can switch among different locomotion modes, such that the robot can choose its mode to adapt complex terrains. To verify the functionality of the robot, we present the results of a series of simulations, and perform the locomotion modes' experiments on a manufactured prototype.

***Index Terms*—Parallel mechanism, folding mechanism, quadruped robot, reconfigurable robot, rolling motion, multiple locomotion modes.**

I. INTRODUCTION

THERE are many classes of mobile robots with different characteristics. Legged robot can achieve walking, crawling, running and jumping by alternatively changing the supporting legs on the ground. This enables it to flexibly explore different environments, but its walking efficiency is lower and the control system is usually very complicated [1-3]. To enhance the walking capability of the robot in different working environments, hybrid robot was presented that constructed by integrating different walking devices together (e.g., wheel-legged robots [4-10], track-legged robots [11], wheel-track-legged robots [12]). But such a combination usually increases the weight and volume of the robot, which makes it less swift [3].

This work has been supported by National Natural Science Foundation of China (51175030), and the Natural Sciences and Engineering Research Council of Canada (NSERC).

Y. B. Tian is with Faculty of Engineering and Applied Science, University of Ontario Institution of Technology (UOIT), Canada. (email:yaobin_tian@yahoo.com)

Dan Zhang, Y. A. Yao and Y. Z. Li are with the School of Mechanical, Electronic and Control Engineering in Beijing Jiaotong University, Beijing 100044, China (e-mail: danzhang@bjtu.edu.cn, yayao@bjtu,edu.cn; 11121434@bjtu.edu.cn).

X. W, Kong is with the Department of Engineering and Physical Sciences, Heriot-Watt University, United Kingdom (email: X.Kong@hw.ac.uk)

* Corresponding author

Different from hybrid robots, several mobile robots can realize different locomotion modes by using reconfigurable methods, which can switch among the locomotion modes of rolling, walking and snake-like crawling, by changing the topology of the robot properly [13-16]. However, the DOFs of a these robots are usually very large, and the modules are required to divide and re-connect to change their locomotion modes. This highly limits the switching speed and increases the control difficulty.

Without modular units, some deformable mobile robots can obtain multiple locomotion modes by deforming their bodies or entire shapes into various topology structures. For example, soft robots composed of multiple loops, can roll, crawl, or jump by changing the shapes of loops [17, 18]. Some legged robots can switch their locomotion modes by deforming the legs into a wheel [19], disk [20] or sphere [21], such that the legged robots can achieve wheeled or spherical rolling motion.

In additional, parallel mechanisms have also been used to realize different locomotion modes (e. g., walking mode [22-24], biped mode [25-28], rolling mode [29-33], crawling mode [34, 35], and worm-like mode [36]). However, the locomotion mode of each of these mobile robots is fixed and the working space is very small, that strictly limits the robot in accommodating different road conditions. To improve the capability of parallel mechanisms, a plenty of parallel mechanisms with multiple operation modes were presented [37, 38]. Several lower DOF parallel robots can realize multiple motion modes, e.g. rotational, translation, planar, or spherical motions etc. Based on different operation modes, we further presented two mobile parallel robots with two different locomotion modes [39, 40]. We also used metamorphic methods to make single loop linkages realize different locomotion modes by changing their gestures. For example, we presented a mobile parallelogram mechanism that can slide or crawl on the ground [41], and used a spatial 8R linkage to realize biped and rolling locomotion [42].

In this paper, we present a parallel robot that can deform into a rolling and quadruped robot, which can significantly improve the capability of a mobile robot. We mainly focus on the mechanical design and the locomotion analysis of the robot. We will show that the robot can be deformed into equivalent open-chain mechanisms or planar closed-loop mechanisms by controlling its singularity positions. Using different mechanisms, this robot can mobile by rolling, tumbling, and quadruped modes. Each of these modes can be quickly switched at its singularity positions for adapting different environments. Furthermore, our robot can be folded into three compact forms, which may be useful for storage or hiding itself

in performing some dangerous tasks.

The rest of the paper is organized as follows. The design and operation modes analysis of the parallel mechanism are introduced in Sec. 2. Section 3 analyzes the different locomotion modes of the robot. Section 4 gives the switching methods of the rolling, tumbling and quadruped modes. Section 5 presents the results of locomotion tests and folding functions on a physical prototype. The conclusions and brief discussions close the paper in Sec. 6.

II. Mechanism Design

In this section, we first introduce the design of the mobile parallel robot. Then, based on the mobility and singularity analysis, we show that the upper platform has four typical operation modes. Using these modes, the robot can be viewed as a parallel manipulator to realize some special movements.

A. Description of mechanism

The proposed robot is illustrated in Figure 1. It is basically a symmetric parallel mechanism with two equal platforms and four equal arms (Figure 1(a)). For ease of description, the two platforms are called the upper platform ($E_1E_2E_3E_4$) and lower platform ($A_1A_2A_3A_4$) respectively, Here E_i and A_i are the endpoints of an arm, and both are R joints with their axes collinear. For the upper platform, $||oA_1|| = ||oA_2|| = ||oA_3|| = ||oA_4||$, and $A_1A_3 \perp A_2A_4$. Each arm consists of five R joints at A_i, B_i, C_i, D_i, and E_i. The positions of R joints on an arm are as follows:

(1) B_i is at the lower left side of A_i with a distance of l_2, and D_i is at the upper left side of E_i with a distance of l_2. In doing so, the R joints at B_i and C_i can be coincident without any physical interfere, and there will be enough space for adding motors and other apparatus.

(2) The axes of three internal R joints B_i, C_i, and D_i are parallel and they are orthogonal to the axes of the end joints A_i and E_i.

(3) $||A_iB_i|| = ||D_iE_i||$, $||B_iC_i|| = ||D_iC_i||$.

The four arms have the same parameters. Table I shows the parameters of the first arm of the robot. In this robot, the total number of R joints is 20 with 12 active and 8 passive joints. The passive joints include 4 R joints at C_i of the four arms and 4 R joints of the two platforms. 12 motors will be used to control corresponding R joints. To clearly show the relations between motors and joints, we used $M_{X,i}$ to denote the Motors, where X,i means the positions marked in Figure 1(a). The positions of motors installed on the robot are shown and marked in Figure 1(b). A real prototype has also been manufactured to show the concept of our robot (see Figure 1(c)).

Table I. Parameters of the robot

Parameter	Description
l_1	Distance of oA_1
l_2	Distance from B_1 to the lower platform
l_3	Length of link A_1B_1
l_4	Length of link C_1D_1

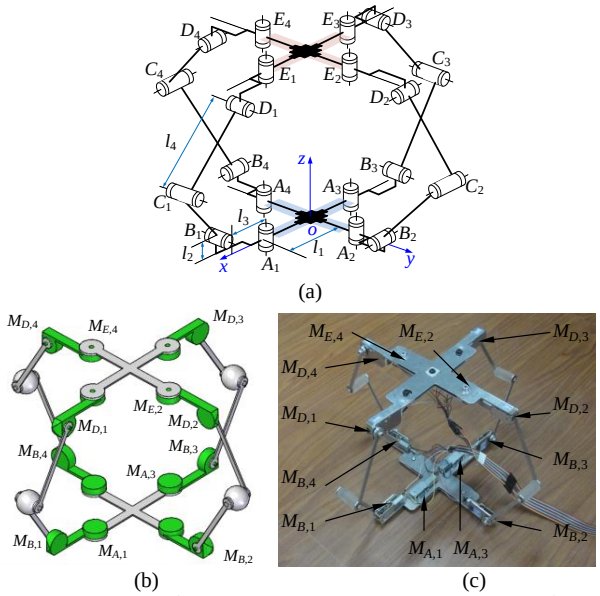

Fig. 1. (a) The sketch of the parallel mechanism, (b) the positions of motors on a 3D model, (c) the prototype of the mechanism.

B. Mobility and operation modes analysis

According to the motions of the upper platform, it can be found using the method [38], that the mechanism has three 4-DOF operation modes at some general configuration. In this section, we mainly consider the practical operation modes, which are subsets of the three general 4-DOF operation modes by locking certain R joints at singular configurations. Based on the singularity [43] and metamorphic [44] characteristics, we get four types of operation modes of the platform. For ease of discussion of the singularity conditions, let R_J denote the axis of R joint J. The relations of two joints are denoted as follows:

$R_J = R_K$, the axes of two R joints J and K are coincident;

$R_J // R_K$, the axes of two R joints J and K are parallel;

$R_J \neq R_K$, the axes of two R joints J and K are not coincident;

$R_J \perp R_K$, the axes of two R joints J and K are perpendicular to each other.

(1) Pure translational motion (T-mode)

Figure 1(a) shows the robot in its T-mode, a coordinate system o-xyz is set up such that its origin is at the center of the lower platform, and x-$axis$ is along oA_1, y-$axis$ is along oA_2. In this moment, the axes of A_i and E_i are collinear and parallel to the z-axis. The four arms are at their singularity positions in the sense that each of them can rotate between the upper and lower platforms about the corresponding line A_iE_i. As shown in Figure 1(b), the rotational motions of four arms are controlled by four motors $M_{A,1}$, $M_{E,2}$, $M_{A,3}$, and $M_{E,4}$ respectively. With the four motors locked, the relative motions between the two platforms are constrained by the four arms. The first and third arms allow the upper platform undergo planar in the xz plane, the second and forth arms allow it undergo planar motion in the yz plane, thus the upper platform can only translate along oz-axis with a single DOF (see Figure 2). This result can also be obtained by screw methods [45]. The working states of 12 motors are given in Table 2. The translational motion of the upper platform are controlled by 8 motors $M_{B,i}$ and $M_{D,i}$ (for i = 1, 2, 3, 4). These 8 motors must be actuated synchronously, and

the rotation directions of $M_{B,i}$ and $M_{D,i}$ are opposite. As shown in Table 2, if $M_{B,i}$ rotate along the positive direction, and $M_{D,i}$ rotate along the negative direction, the upper platform will be lifted up.

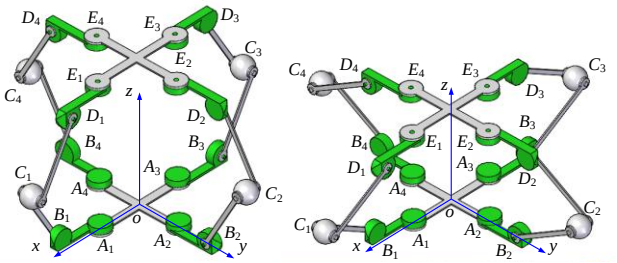

Fig. 2. Pure translational motion of the platform.

Table 2. Working states of motors in T-mode.

Motion	Motors	Working States
T-mode	$M_{A,1}$, $M_{E,2}$, $M_{A,3}$, $M_{E,4}$,	○
	$M_{B,i}$, (for i = 1, 2, 3, 4)	⊕ / ⊖
	$M_{D,i}$, (for i = 1, 2, 3, 4)	⊖ / ⊕

○ independently

⊕ synchronously (positive direction)

⊖ synchronously (negative direction)

(2) Plane motion (P-mode)

Considering the arms' rotational motions in T-mode, if the four arms are at the state when all the axes of $R_{B,i}$, $R_{C,i}$, and $R_{D,i}$ are parallel, the mechanism may deform into a planar state. As shown in Figure 3, let four arms rotate by angles of ϕ_1, ϕ_2, ϕ_3, and ϕ_4 from their initial position (dashed lines in Figure 3(b)) respectively, and the range of ϕ_i is (–90 90) deg. If $\phi_1 = \phi_3$, $\phi_2 = \phi_4$, and $|\phi_1| + |\phi_2| = 90$ deg (see in Fig, 3(b)), the axes of $R_{B,i}$, $R_{C,i}$, and $R_{D,i}$ must be parallel. In this case, the mechanism can be viewed as an equivalent planar 10-bar and 12R linkage (see the side view in Fig. 3(c)). Using G-K conditions, the DOF can be calculated as: $M = 3 \times 9 - 2 \times 12 = 3$. The upper platform has 3-DOF motions (one rotational and two translational motions) in the shaded plane (see in Figure 3(a)). Adding the rotational motions of four arms, the total number of DOFs is 7. However, if the upper platform moves to the left or to the right, that causes the axes of $R_{A,i}$ and $R_{E,i}$ to be not collinear, all the four arms cannot rotate anymore, and the DOFs will be decreased to three.

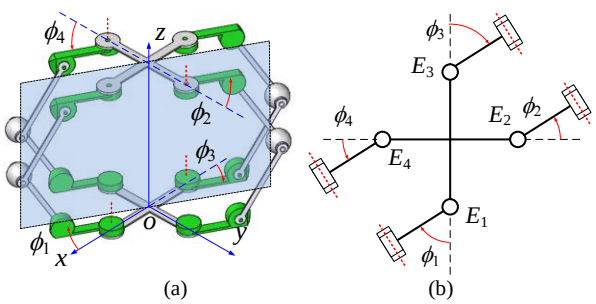

(a) (b)

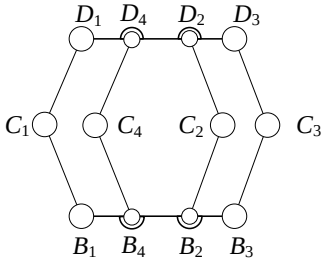

(c)

Fig. 3. Planar states of the mechanism: (a) a general view of the mechanism, (b) a top view of the sketch, (c) a side view of the sketch

Depending on the collinear of the axes of R joint on the arms, we have the following two cases:

Case 1: Two pairs of the arms' R joints are collinear.

When $|\phi_1| = |\phi_2| = 45$ deg, as shown in Figure 4, there are two configurations. In the first one, the axes of three middle R joints of the first and fourth arms are collinear respectively, i.e., $R_{B,1} = R_{B,4}$, $R_{C,1} = R_{C,4}$, and $R_{D,1} = R_{D,4}$; $R_{B,2} = R_{B,3}$, $R_{C,2} = R_{C,3}$, and $R_{D,2} = R_{D,3}$. In the second one, $R_{B,1} = R_{B,2}$, $R_{C,1} = R_{C,2}$, and $R_{D,1} = R_{D,2}$; $R_{B,3} = R_{B,4}$, $R_{C,3} = R_{C,4}$, and $R_{D,3} = R_{D,4}$. Taking the first configuration as an example, the resulting state of the mechanism is shown in Figure 5(a). The side view of it is shown in Figure 5(b). Then, we shall lock the four motors $M_{A,1}$, $M_{A,3}$, $M_{E,2}$, and $M_{E,4}$, such that the joints of $R_{A,i}$ and $R_{E,i}$ are locked. In the view of metamorphic [44], this state can be considered as an equivalent planar 6R closed-loop linkage (see Figure 3(c)). Similarly, in the second configuration, the mechanism can also be considered as another 6R linkage.

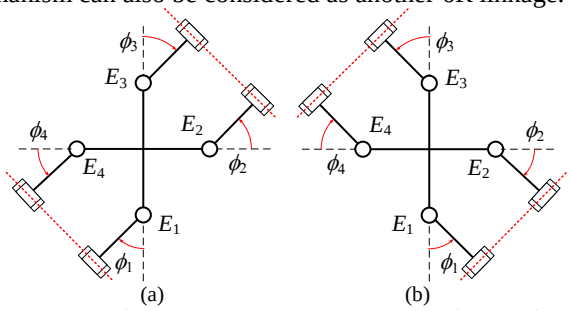

(a) (b)

Fig. 4. Two pairs of arms' R joints are collinear: (a) the first and fourth (the second and third) arms are collinear, (b) the first and second (the third and fourth) arms are collinear.

Case 2: One pair of the arms' R joints is collinear.

As shown in Figure 6, there are two configurations. In the first one, $\phi_1 = \phi_3 = 0$ deg, $|\phi_2| = |\phi_4| = 90$ deg; and in the second one, $\phi_2 = \phi_4 = 0$ deg, $|\phi_1| = |\phi_3| = 90$ deg. The resulting state of the mechanism corresponding to the first one is shown in Figure 6(a). Using the same method, it can be viewed as an equivalent planar 8-bar mechanism.

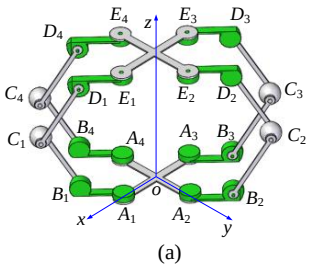

(a)

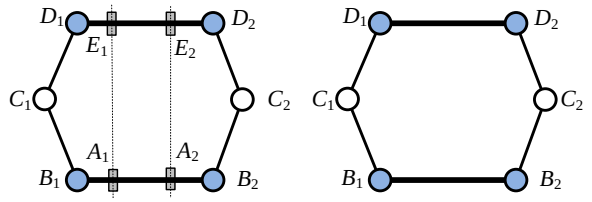

Fig. 5. (a) Deform into a planar mechanism, (b) a side view of the mechanism, (c) an equivalent planar 6R linkage.

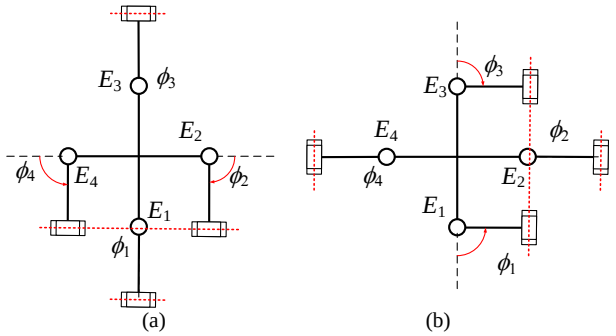

Fig. 6. One pair of arms' R joints is collinear: (a) the second and fourth arms are collinear, (b) the first and third arms are collinear.

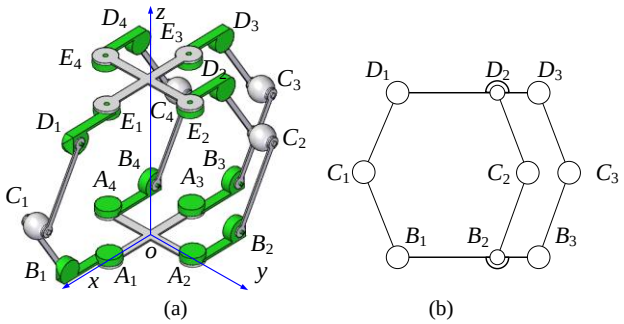

Fig. 7. (a) Deform into a planar mechanism on the *yz* plane, (b) an equivalent planar 8-bar mechanism.

Based on the above description, during P-mode, the four arms are locked. For the motors at the coincident joints, they need to be actuated synchronously. The details of 12 motors' working states in P-mode are shown in Table 3.

Table 3. Working states of motors in P-mode.

P-mode	Motors	Working States
Each case	$M_{A,1}$, $M_{E,2}$, $M_{A,3}$, $M_{E,4}$,	⊗
Case 1: (a)	$M_{B,1}$ and $M_{B,4}$ $M_{D,1}$ and $M_{D,4}$ $M_{B,2}$ and $M_{B,3}$ $M_{D,2}$ and $M_{D,3}$	◎
Case 1: (b)	$M_{B,1}$ and $M_{B,2}$ $M_{D,1}$ and $M_{D,2}$ $M_{B,3}$ and $M_{B,4}$ $M_{D,3}$ and $M_{D,4}$	◎
Case 2: (a)	$M_{B,2}$ and $M_{B,4}$ $M_{D,2}$ and $M_{D,4}$	◎
Case 2: (b)	$M_{B,1}$ and $M_{B,3}$ $M_{D,1}$ and $M_{D,3}$	◎

⊗ locked

◎ synchronously

(3) Pure rotational motion (R-mode)

Consider the planar 6R configuration in Figure 3, when B_2, D_2, B_3, and D_3 are coincident, we have a new state as shown in Figure 8. At this state, the upper platform has only one rotational motion about line B_2D_2. As shown in Figure 8(b), the second and third arms are deformed into an equivalent single link respectively. Each of the equivalent links can be controlled by the corresponding two motors, e. g., link B_2C_2 is controlled by motors $M_{B,2}$ and $M_{D,2}$ which should be actuated synchronously with the same direction. From the side view of the sketch, the two platforms construct an equivalent 4R linkage. Thus, the DOF of the upper platform will be one. Considering the two free links B_2C_2 and B_3C_3, the total FOF of the mechanism are three. Similarly, if B_1 and D_1 are coincident, the upper platform will rotate about line B_1D_1. Since there are two planar 6R configurations, the upper platform has four rotational directions (i.e., u_1, u_2, u_3, and u_4) as shown in Figure 8(c). The working states of 12 motors in R-mode are shown in Table 4.

Table 4. Working states of motors in R-mode.

R-mode	Motors	Working States
Each u_i	$M_{A,1}$, $M_{E,2}$, $M_{A,3}$, $M_{E,4}$,	⊗
Rotating about u_1	$M_{B,1}$ and $M_{B,4}$ $M_{D,1}$ and $M_{D,4}$	Ⓢ
	$M_{B,2}$ and $M_{B,3}$ $M_{D,2}$ and $M_{D,3}$	Ⓞ
Rotating about u_2	$M_{B,2}$ and $M_{B,3}$ $M_{D,2}$ and $M_{D,3}$	Ⓢ
	$M_{B,1}$ and $M_{B,4}$ $M_{D,1}$ and $M_{D,4}$	Ⓞ
Rotating about u_3	$M_{B,3}$ and $M_{B,4}$ $M_{D,3}$ and $M_{D,4}$	Ⓢ
	$M_{B,1}$ and $M_{B,2}$ $M_{D,1}$ and $M_{D,2}$	Ⓞ
Rotating about u_4	$M_{B,1}$ and $M_{B,2}$ $M_{D,1}$ and $M_{D,2}$	Ⓢ
	$M_{B,3}$ and $M_{B,4}$, $M_{D,3}$ and $M_{D,4}$	Ⓞ

⊗ locked

Ⓢ synchronously (same direction)

Ⓞ synchronously (opposite direction)

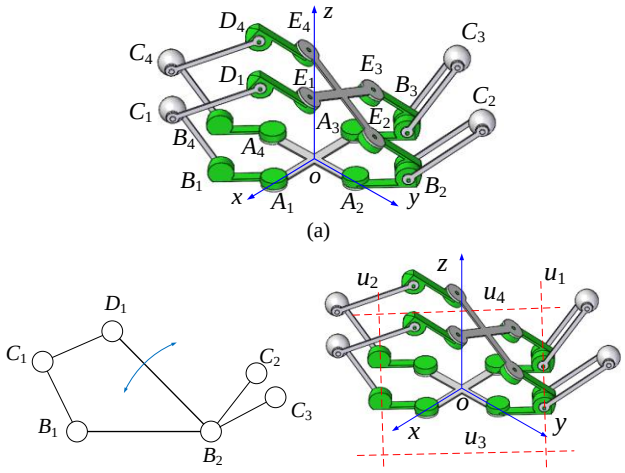

Fig. 8. (a) Pure rotation motion, (b) an equivalent planar four-bar mechanism, (c) the rotation directions.

(4) Lock-up motion (L-mode)

During the T-mode, if the upper platform is moving down to the base one, when all $R_{B,i}$ and $R_{D,i}$ are coincident as shown in Figure 9(a), each of the four arms is at a spatial singularity position. At this moment, the two motors at $R_{B,i}$ and $R_{D,i}$ can be actuated synchronously (the same direction or opposite directions). If the two motoes are in opposite directions, the upper platform will be lifted up. If the motors' directions are the same, links B_iC_i and C_iD_i will be controlled as a single link. In this case, each arm is folded into an equivalent serial arm with 2-DOF (see Figure 9(b)). That also leads the two platforms to be locked together. The DOF of the robot will be eight. The working states of 12 motors in L-mode are shown in Table 5.

Table 5. Working states of motors in L-mode.

L-mode	Motors	Working States
L-mode	$M_{A,1}$, $M_{E,2}$, $M_{A,3}$, $M_{E,4}$	○
	$M_{B,1}$ and $M_{D,1}$	Ⓢ
	$M_{B,2}$ and $M_{D,2}$	Ⓢ
	$M_{B,3}$ and $M_{D,3}$	Ⓢ
	$M_{B,4}$ and $M_{D,4}$	Ⓢ

○ independently

Ⓢ synchronously (same direction)

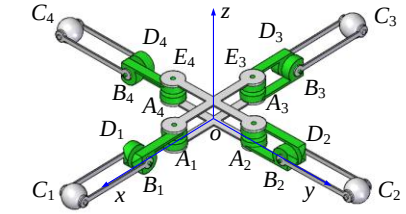

(a)

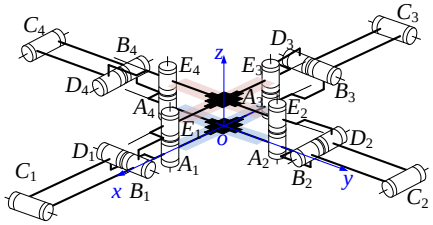

(b)

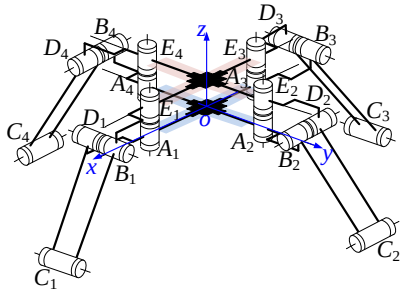

(c)

Fig. 9. (a) The upper platform is fixed with lower platform, (b) switching position, (c) an equivalent four legged robot.

(5) Switching states

Based on the motions analysis of the upper platform, we have obtained four typical modes. According to their positions, we give a general sketch of the relations of the four modes (see Fig. 10). One mode can be changed into the other modes via some special states. We call these states switching states, which are the singularity positions of the mechanisms. The singularity positions can be obtained when some axes of R joints are coincident. As shown in Table 6 in Appendix, we show the details motions of the upper platform and the conditions of the singularity positions. The figures in Table 6 are also the switching states, at which the motions of mechanism can be changed to other modes. Based on it, we can find the rapid way to switch the motion modes. For example, the T-mode and L-mode can be switched freely at any position.

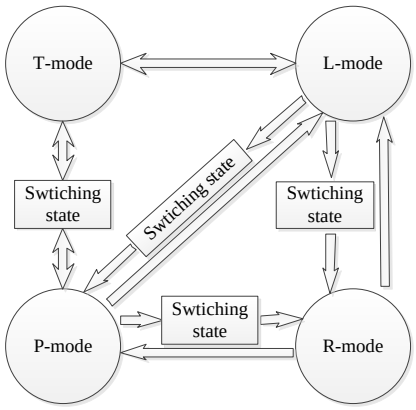

Fig. 10. The switching functions of the motion modes.

III. Locomotion Modes Analysis

In this section, based on the four operation modes presented in Section 2, we will use different equivalent mechanisms to establish rolling, tumbling and quadruped locomotion modes. The simulations are also performed based on a computational 3D-model to show the locomotion modes.

A. Rolling locomotion

Rolling is a very efficient manner of locomotion on flat ground. Yim et al. first introduced a kind of locomotion modes called tracked-rolling with a plenty of modules [13]. Sastra et al. further presented a fast and efficient rolling gait based on a closed-loop mechanism with numbers of modules [46]. Liu et al. [47] and Yamawaki et al. [33] designed mobile robots with rolling functions with planar 4R and 5R closed-loop mechanisms respectively. Each of such rolling robots changes the shapes of its loop (and therefore the position of its mass center) such that it can roll on the ground by changing its supporting edge (foot) alternatively.

Based on the analysis in section 2.2, during the P-mode, the mechanism can be deformed into a single-loop 6R linkage (see Figure 5). Our purpose is to realize rolling locomotion by changing the shape of the loop.

Note that the DOF of the 6R linkage is three, we can use four pairs of motors to control the 6R linkage in Figure 11(a): (i) $M_{B,1}$ and $M_{B,4}$ to control α, (ii) $M_{D,1}$ and $M_{D,4}$ to control β, (iii) $M_{B,2}$ and $M_{B,3}$ to control γ, (iv) $M_{D,2}$ and $M_{D,3}$ to control δ. Among the four pairs of motors, one pair of motors is redundant. To simplify the control method, we shall let $\alpha = \delta$, and $\beta = \gamma$ for symmetry reason. Then, the configuration of linkage is determined by only two independent variables (α and γ, see Figure 11(b)). Due to the symmetric configuration, $C_1D_1C_2B_2$ is

a parallelogram, and the motors are mounted at the vertexes of the loop, the center of the mass can be considered nearly at the center of the geometric shape.

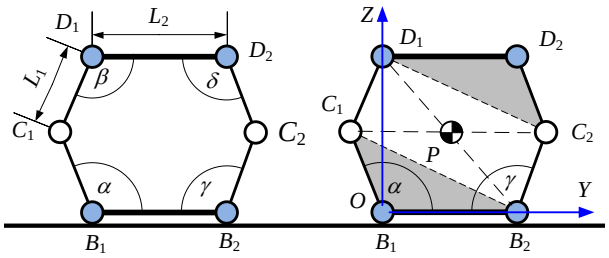

(a) (b)

Fig. 11. The sketch of the 6R linkage.

As shown in Figure 11(b), a new coordinate system *O-XYZ* is set at point B_1 with Y-axis passing point B_2 and Z-axis along the vertical direction. Let L_1 be the length of B_1C_1, and $L_1 = l_4$; let L_2 be the length of B_1B_2, and $L_2 = \sqrt{2}\, l_1 + 2l_3$. For a given set of input angles α and γ, the positions of C_1 and C_2 can be expressed as

$$\mathbf{r}_{C1} = \begin{bmatrix} 0 & L_1\cos\alpha & L_1\sin\alpha \end{bmatrix}^T \quad (1)$$

$$\mathbf{r}_{C2} = \begin{bmatrix} 0 & L_2 - L_1\cos\gamma & L_1\sin\gamma \end{bmatrix}^T \quad (2)$$

Since the center of the loop is at the middle of $C_1D_1C_2B_2$, the center of the mass ($\mathbf{r}_P$) can be expressed as

$$\mathbf{r}_P = \frac{1}{2}\left(\mathbf{r}_{C1} + \mathbf{r}_{C2}\right) = \frac{1}{2}\begin{bmatrix} 0 \\ L_2 + L_1\cos a - L_1\cos\gamma \\ L_1\left(\sin a + \sin\gamma\right) \end{bmatrix} \quad (3)$$

Using the kinematic rolling principle (Sastra, 2009), the rolling locomotion can be realized by changing the shapes of the loop as well as the positions of $\mathbf{r}_P$. Figure 12 shows a rolling cycle to the right. A rolling cycle contains the following steps:

(a) Refer to the state in Figure 11(a), let $\alpha = \gamma = 90$ deg, $\beta = \delta = 90$ deg (as shown in Figure 12(a)), it is a rectangular shape, and we define this position as the initial state. At this moment, $r_{P,x} = 0.5L_2$. Then, increasing γ, $r_{P,x}$ will move to the right.

(b) When $\gamma = 180$ deg, point C_2 is on the ground, and let γ be unchanged. At this state, $r_{P,x} = 0.5(L_2 + L_1)$. Then, decreasing α, the mechanism can be viewed as a parallelogram, and $r_{P,x}$ will move to point B_2.

(c) When α reaches the following angle (α^*),

$$\alpha^* = \arccos\left(\left(L_2 - L_1\right)/L_1\right) \quad (4)$$

One learns from Eq. (3) that $r_{P,x}$ is coincident with point B_2, and $r_{P,x} = L_2$. According to the trigonometric functions, we have $L_2 < 2L_1$. Using $L_2 = \sqrt{2}\, l_1 + 2l_3$, $L_1 = l_4$, the length of the mechanism must satisfy

$$l_4 > l_3 + l_1\sqrt{2}/2 \quad (5)$$

(d) If $\alpha < \alpha^*$, $r_{P,x}$ is in the range of B_2C_2. Then, by decreasing γ and increasing α, point B_1 will be pulled away from the ground, and point D_2 will be pushed down to the ground. That means the mechanism can be supported by link B_2C_2.

(e) When γ is decreased at an angle that $\alpha + \gamma = 180$ *deg*, point D_2 will be on the ground, and the arm ($B_2C_2D_2$) will support the mechanism.

(f) When $\alpha = \gamma = 90$ *deg*, the shape of the loop is a rectangle, and $r_{P,x} = L_2 + L_1$. In this configuration, links B_1D_1 and B_2D_2 are perpendicular to B_1B_2, thus the axes of R joints $R_{A,i}$ and $R_{E,i}$ must be coincident. Refer to the T-mode in section 2.2, this mechanism is at a switching state.

(g) Increasing α and decreasing γ synchronously with the same angular velocity, the shape of the loop remain to be parallelogram, and $r_{P,x}$ will move in the range of link C_2D_2.

(h) When γ is decreased to the same value as α^*, and $\alpha = 180 - \gamma$, then fix γ. Only α is being increased. That will pull point B_2 away from the ground, and push point D_1 down to the ground.

(i) When $\alpha = 180$ deg, and $\gamma = \alpha^*$, due to symmetric, the shape is similar to the configuration in step (c). At this moment, $r_{P,x}$ is coincident with point D_2, and $r_{P,x} = L_2 + 2L_1$. Then, increasing γ, $r_{P,x}$ will move into the range of link D_2D_1.

(j) When $\gamma = 90$ deg, $\alpha = 180$ deg, the state of the mechanism is similar with the configuration in step (b). Then, decreasing α, point C_2 will be pulled away from the ground.

(k) When $\alpha = \gamma = 90$ deg, the mechanism returns back to a position similar to the initial state, and $r_{P,x} = 1.5L_2 + 2L_1$. Till now, a rolling cycle is completed. Using the same process, the loop can roll to one side continually.

Using the steps (a-k), Figure 13 gives an example of the curves of input angles (As an example, the angles are changed with a fixed angular velocity). From the curves in Figure 13, we can see that, except the steps (e-g), only one variable is changed. The input angles are symmetric with the state in Figure 13(f), i.e., the curve of α in steps (a-f) is the same with γ in steps (f-k). That will significantly simplify the control program, and save the energy. A simulation of the rolling cycle in a general view is shown in Figure 14. For the first configuration in Figure 14, it is a general position of the mechanism in T-mode. The mechanism has to deform its state into the rolling mode. Then, using the gaits in Figure 12, a rolling locomotion is simulated by a computer. Referring to the 6R linkage, there are two different planar states. Therefore, we have two rolling directions at each state of the 6R linkage, and the directions can be changed freely by adjusting the arms' positions (see Figure 15).

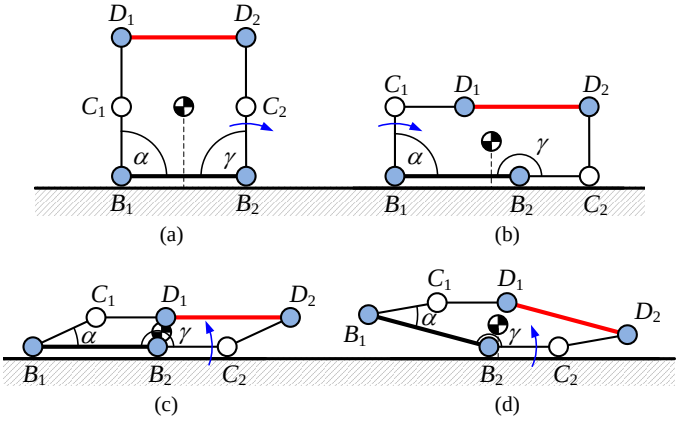

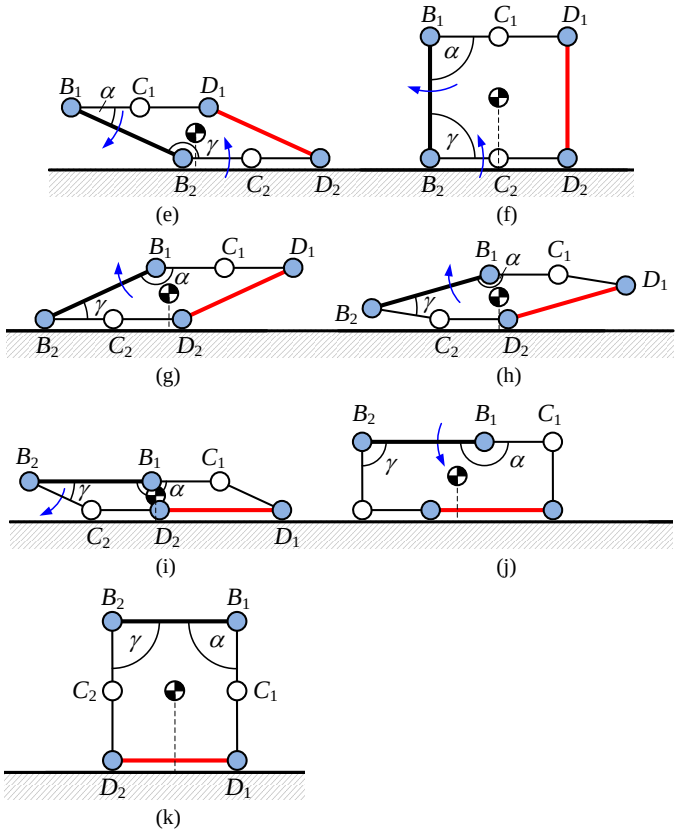

Fig. 12. The rolling locomotion mode.

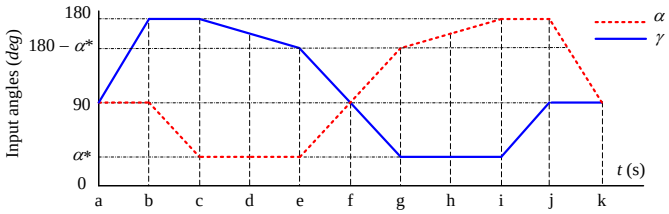

Fig. 13. Variation of input angles in a rolling cycle.

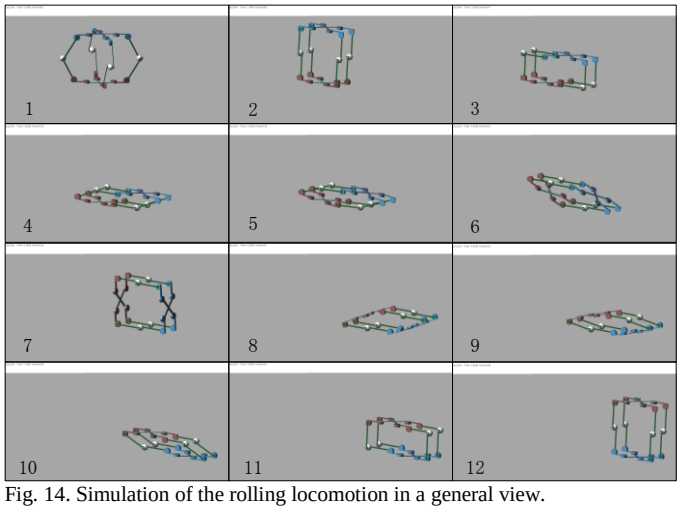

Fig. 14. Simulation of the rolling locomotion in a general view.

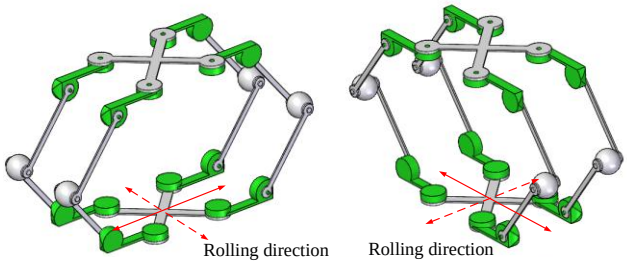

Fig. 15. Rolling directions of the mechanism.

B. *Tumbling locomotion*

As shown in Figure 16(a), the mechanism is in a configuration in which two arms support the mechanism. This position is also a part of the T-mode of the robot mentioned in Figure 2. As shown in Figure 16(b), the distance of the two platforms can be changed freely with T-mode. Choosing $M_{A,1}$, $M_{A,3}$, $M_{E,2}$ and $M_{E,4}$ as working motors, and if $M_{D,i}$ and $M_{B,i}$ (for all i) are locked, in the view of metamorphic, each arm can be viewed as a single rigid link which can rotate about A_i and E_i between the platforms. Using this function, a tumbling locomotion can be obtained. It is equivalent to a 4-DOF planar 5-bar open-chain mechanism. The sketch of the mechanism is shown in Figure 16(c).

Using the sketch of the mechanism, Figure 16 shows the critical steps of making a tumble to the right (the tumbling steps to the left can be performed similarly). Essentially, it is realized by rotating proper arms alternatively as indicated by the arrows. A similar tumbling locomotion can be found in ref. [48]. First, we analyze the tumbling conditions, then, the tumbling motion is introduced.

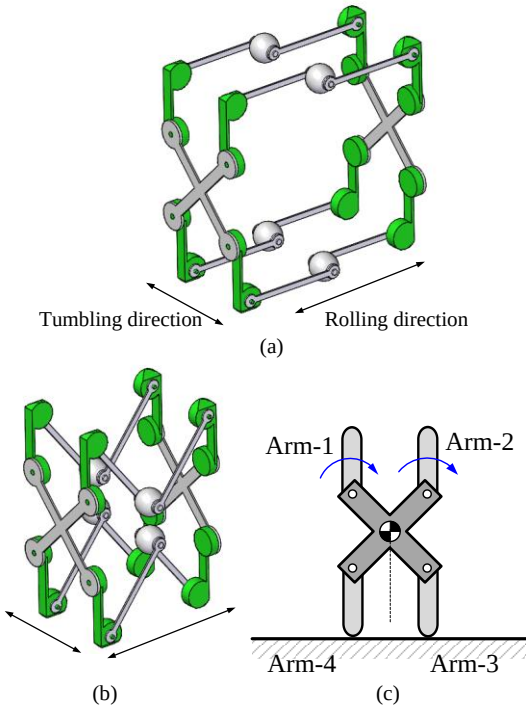

Fig. 16. (a) A switching state between P-mode and T-mode, (b) adjusting its width, (c) the sketch of the mechanism.

(1) Tumbling condition

Figure 17 is a simplified sketch of the five-bar mechanism. The crossing link is platform. Four links A_iB_i (i = 1, 2, 3, 4) are the arms. A coordinate system O-XY is set at the centre of the platform, and a global coordinate system O_1-X_1Y_1 is set at point B_3. The input angles of the four arm are defined as θ_i (i = 1, 2, 3, 4). According to the structure, point A_i and B_i can be expressed as

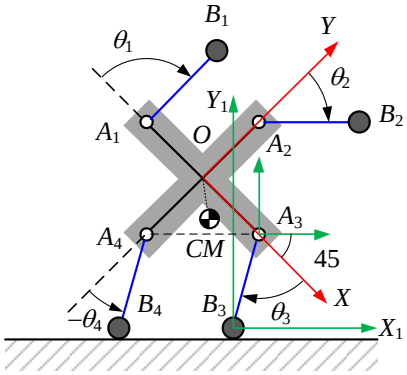

Fig. 17. A sketch of the five-bar linkage.

$$\begin{aligned}&\mathbf{r}_{A1}=\begin{bmatrix}-l_1 & 0\end{bmatrix}^T,\mathbf{r}_{A2}=\begin{bmatrix}0 & l_1\end{bmatrix}^T\\&\mathbf{r}_{A3}=\begin{bmatrix}l_1 & 0\end{bmatrix}^T,\mathbf{r}_{A4}=\begin{bmatrix}0 & -l_1\end{bmatrix}^T\end{aligned}\tag{6}$$

$$\begin{cases}\mathbf{r}_{B1}=\begin{bmatrix}-l_1-l_3\cos\theta_1 & -l_3\sin\theta_1\end{bmatrix}^T\\\mathbf{r}_{B2}=\begin{bmatrix}-l_3\sin\theta_2 & l_1+l_3\cos\theta_2\end{bmatrix}^T\\\mathbf{r}_{B3}=\begin{bmatrix}l_1+l_3\cos\theta_3 & l_3\sin\theta_3\end{bmatrix}^T\\\mathbf{r}_{B4}=\begin{bmatrix}l_3\sin\theta_4 & -l_1-l_3\cos\theta_4\end{bmatrix}^T\end{cases}\tag{7}$$

Due to symmetry, let A_i has a mass m_1, and B_i has a mass m_2. Then, the centre of mass of the mechanism can be expressed as

$$\mathbf{r}_{CM}=\frac{l_3m_2}{4(m_1+m_2)}\begin{bmatrix}\cos\theta_1-\cos\theta_3+\sin\theta_2-\sin\theta_4\\\cos\theta_2-\cos\theta_4-\sin\theta_1+\sin\theta_3\end{bmatrix}\tag{8}$$

To make the mechanism tumble, the $r_{CM,\,X1}$ need to be out of the supporting area (B_4B_3). Further, at the beginning, link A_3B_3 and A_4B_4 are parallel, i.e., A_4A_3 // B_4B_3, and $|\theta_3|+|\theta_4|=90$ deg. In this case, the platform can only have translational motion in X_1Y_1 plane before it tumbles. Using this, we can get the transform relations between $\{O_1\}$ and $\{O\}$. Let $\{A_3\}$ be the middle coordinate system at point A_3. The transform matrix can be expressed as follow:

$${}^{O1}T_{A3}=Trans(k_1,k_2)=\begin{bmatrix}1&0&k_1\\0&1&k_2\\0&0&1\end{bmatrix}\tag{9}$$

Where $k_1=l_3\sin(-\theta_3-45°)$ $k_2=l_3\cos(-\theta_3-45°)$

$$\begin{aligned}{}^{A3}T_O&=Rot(Z,-45°)Trans(-l_1)\\&=\begin{bmatrix}k_3&k_3&-l_1k_3\\-k_3&k_3&l_1k_3\\0&0&1\end{bmatrix}\end{aligned}\tag{10}$$

where $k_3=\sqrt{2}/2$.

Using Eq. (9) and Eq. (10), ${}^{O1}T_O$ can be written as

$${}^{O1}T_O=\begin{bmatrix}k_3&k_3&-l_1k_3+k_1\\-k_3&k_3&l_1k_3+k_2\\0&0&1\end{bmatrix}\tag{11}$$

According to Eq. (8) and Eq. (11), the $\mathbf{R}_{CM}$ in the global system is

$${}^{O1}R_{CM}=\begin{bmatrix}k_3r_{CM,x}-k_3r_{CM,y}-l_1k_3+k_1\\k_3r_{CM,x}+k_3r_{CM,y}+l_1k_3+k_2\\1\end{bmatrix}\tag{12}$$

$\mathbf{R}_{CM}$ can be expressed as

$$\mathbf{R}_{CM}=\begin{bmatrix}l_3\sin(-\theta_3-45°)-l_1k_3-f(\theta_1,\theta_2,\theta_3,\theta_4)\\l_3\cos(-\theta_3-45°)+l_1k_3+f(\theta_1,\theta_2,\theta_3,\theta_4)\end{bmatrix}\tag{13}$$

Where

$$\begin{aligned}&f(\theta_1,\theta_2,\theta_3,\theta_4)=\\&\frac{m_2k_3l_3}{4(m_1+m_2)}(\cos\theta_1+\cos\theta_2-\cos\theta_3-\cos\theta_4\\&-\sin\theta_1+\sin\theta_2+\sin\theta_3-\sin\theta_4)\end{aligned}$$

At the state in Figure 17, the tumbling conditions can be obtained as follow:

$$\begin{cases}R_{CM,x}>0\\R_{CM,x}<-\sqrt{2}l_1\end{cases}\tag{14}$$

where the first equation is the tumbling condition to the right, and the second one is the condition to the left.

(2) Tumbling gait

Take the tumbling locomotion to the right as an example, we show the basic gaits in a tumbling cycle. Note that, the state in Figure 16(a) is a switching state of rolling and tumbling mode. We define this position as the initial state. Figure 18 is a tumbling cycle of the five-bar mechanism, the corresponding curves of input angles are shown in Figure 19. Based on that, a simulation of the tumbling locomotion in a general view using the gaits in Figure 18 is shown in Figure 20. The detail of the tumbling gaits is as follows:

(a) At the initial state, $\theta_1=\theta_3=-45$ deg, $\theta_2=\theta_4=45$ deg, and $R_{CM,x}=-l_1\sqrt{2}/2$.

(b) Let points B_1 and B_2 are at their rightmost positions, i.e., $\theta_1=-135$ deg, $\theta_2=-45$ deg. To make the mechanism tumble to right, $R_{CM,x}>0$. If A_3B_3 // A_4B_4, the platform A will have no rotational movements. Then, we can let $|\theta_3|+|\theta_4|=90$ deg (rolling to the right, $-\theta_3+\theta_4=90$ deg; rolling to left, $\theta_3-\theta_4=90$ deg). Eq. 13 can be re-written as

$$\mathbf{R}_{CM}=\begin{bmatrix}l_3\sin(-\theta_3-45°)-l_1k_3-g(\theta_1,\theta_2,\theta_3)\\l_3\cos(-\theta_3-45°)+l_1k_3+g(\theta_1,\theta_2,\theta_3)\end{bmatrix}\tag{15}$$

Where

$$\begin{aligned}&g(\theta_1,\theta_2,\theta_3)=\frac{m_2k_3l_3}{4(m_1+m_2)}(\cos\theta_1+\cos\theta_2\\&-2\cos\theta_3-\sin\theta_1+\sin\theta_2)\end{aligned}$$

According to tumbling condition, using Eq. 15, the angle θ_3 can be computed by Eq. (16). Once $R_{CM,x}$ is out of the supporting area, the mechanism will roll about point B_3. Point B_4 will be away from the ground immediately, and point B_2 will be on the ground at last.

$$l_3 \sin(-\theta_3 - 45°) - \frac{\sqrt{2}}{2} l_1 + \frac{\sqrt{2} m_2 l_3 \cos\theta_3}{4(m_1 + m_2)} > 0 \quad (16)$$

(c) When B_2 is on the ground, controlling the three angles θ_1, θ_3, and θ_4 to make the mechanism stand by B_2 and B_3.

(d) When $\theta_1 = \theta_3 = -45$ deg, $\theta_2 = \theta_4 = 45$ deg, the mechanism returns back to a similar initial state.

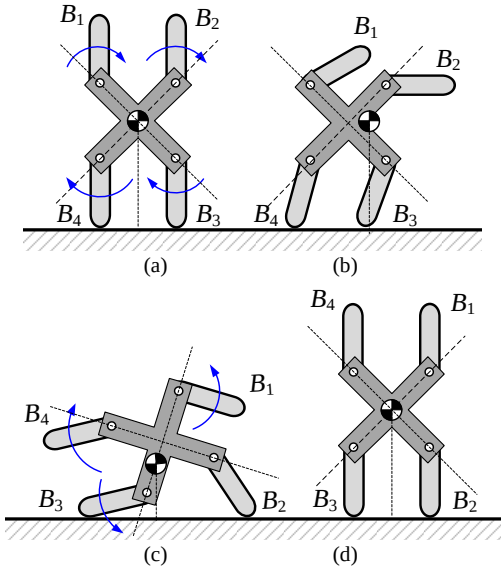

Fig. 18. The tumbling locomotion mode.

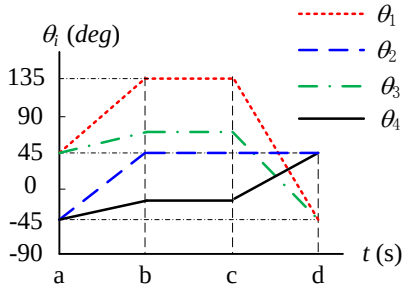

Fig. 19. The curves of input angles in a tumbling cycle.

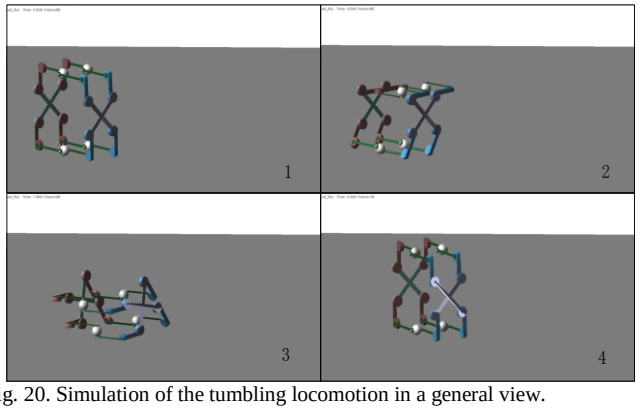

Fig. 20. Simulation of the tumbling locomotion in a general view.

According to the tumbling and rolling mode, we consider that the main benefits of the two modes are:

(1) Changing the directions

Node that, we have discussed that rolling mode and tumbling mode have a common switching state but different moving directions, therefore, the two modes can be changed freely at their switching states, as well as the moving directions.

(2) Rescuing the robot

Generally, mobile robots will hardly get their mobile abilities back when robots fall down. For example, the wheels or tracks cannot touch ground, robots will lose the forces. So, we point out that the tumbling mode will help robot move on when it falls down or other locomotion modes are failure.

C. *Quadruped mode*

See Figure 9(a, b), since the axes of $R_{B,i}$ and $R_{D,i}$ are collinear, each arm can be viewed as a 2-DOF linkage. Lifting each arm about B_i will result in a state of the robot with four legs. See Fig. 9(c) for an illustration of the four-leg robot in a standing state. Particularly, A_i and E_i can be viewed as a hip joint, B_i and D_i can be viewed as a knee joint, C_i can be viewed as a foot (touching the ground). To control the four-leg robot to walk properly, motors $M_{A,1}$, $M_{A,3}$, $M_{E,2}$, and $M_{E,4}$ will drive the four hip joints respectively; motors $M_{B,i}$ and $M_{D,i}$ will drive the knee joints with the same speed and direction. Fig. 21 is the sketch of an equivalent leg, let σ_1 and σ_2 be the input angles of hip and knee joints respectively. The D-H parameters are given in Table 7. Using D-H method, the position matrix of C_3 can be expressed as Eq. (16). Then, $\mathbf{r}_{C3}$ can be written as Eq. (17). Using the parameters in Table 8, the workspace of one single foot is obtained as shown in Figure 22.

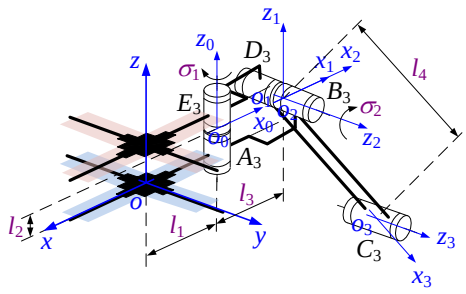

Fig. 21. The sketch of an equivalent single leg.

Table 7. D-H parameters.

A_i	A_1	A_2	A_3	A_4
a_i	l_1	l_3	0	l_4
α_i	180	0	90	0
d_i	l_2	0	0	0
σ_i	0	σ_1	0	σ_2

$$\mathbf{r}_{c_3} = \begin{bmatrix} -l_3\cos\sigma_1 - l_4\cos\sigma_1\cos\sigma_2 - l_1 \\ -l_3\sin\sigma_1 - l_4\sin\sigma_1\cos\sigma_2 \\ l_4\sin\sigma_2 + l_2 \end{bmatrix} \quad (17)$$

Table 8. An example of the structure parameters.

l_1 (mm)	l_2 (mm)	l_3 (mm)	l_4 (mm)	σ_1 (deg)	σ_2 (deg)
100	20	100	200	(-90, 90)	(-150, 150)

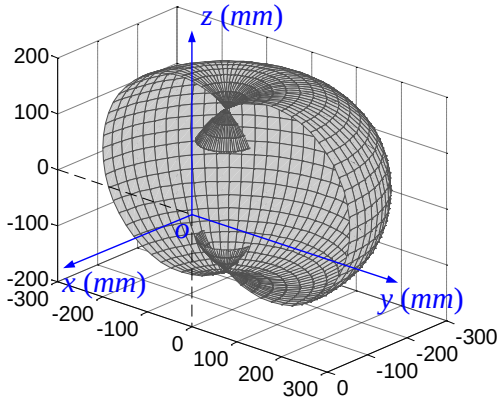

Fig. 22. The workspace of a foot.

Siciliano and Khatib [49] provided the typical gaits of four-leg walking animals. Further, Hirose et al. [50] presented the walking gaits of four-leg robots based on the approach of *static walk*. The principle of static walk is to control the four feet of the robot such that the projection of the mass center is always lying in the supporting area. Here a supporting area is a triangle or a quadrilateral formed by connecting the feet on the ground. Fig. 23 shows a simulation process based on the static walk principle. The walking direction is shown with a dashed arrow. The left of each figure is a general view, and the right one is the top view. Note that, during this walking cycle, we let the body (two platforms) be parallel with the ground. The detail of the walking gaits is as follows:

(a) An initial state with four feet on the ground. C_3 can be lifted up (by a rotation about its knee B_3) and swung along clockwise (by a rotation about its hip A_3). Thus, $C_1C_2C_4$ will support the mechanism.

(b) C_3 is lowered down to touch the ground. C_2 can be lifted up and swung along clockwise. Thus, $C_1C_3C_4$ will support the mechanism.

(c) C_2 is lowered down to touch the ground. C_4 can be lifted up and swung along anti-clockwise. Thus, $C_1C_2C_3$ will support the mechanism.

(d) C_4 is lowered down to touch the ground. C_1 can be lifted up and swung along anti-clockwise. Thus, $C_2C_3C_4$ will support the mechanism.

(e) C_1 is lowered down to touch the ground, and $C_1C_2C_3C_4$ will support the mechanism. Rotating the four legs, the platform will be pushed forward.

(f) Each of the four legs reaches at the initial position. A walking cycle is completed.

Based on the above description, to make the robot continually walk along the given direction, the orders of working legs are C_3-C_2-C_4-C_1. Choosing different orders of legs, the walking directions can also be changed freely.

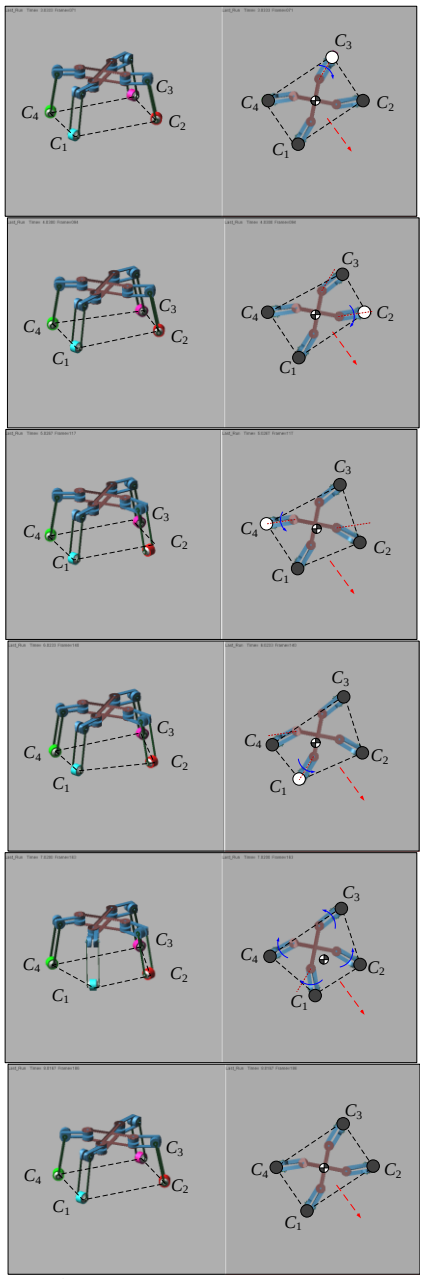

Fig. 23. Simulation of walking locomotion, the dashed polygon is the supporting region obtained by connecting the feet on the ground.

According to the above analysis, we give a general comparison of three locomotion modes as shown in Table 9. Tumbling mode has the 4 DOFs and four working motors, and each of the motors can be controlled independently. But the mobile direction cannot be changed. Rolling mode has the lowest DOFs and 8 working motors. It can be operated by redundant control method. Motors must be actuated synchronously and satisfied rolling conditions. The rolling directions can be changed at the state in Fig. 15. Quadruped mode has 8 DOFs and 12 working motors. The two motors at the knee joints have to be actuated synchronously. I can be walked to any directions on the ground.

Table 9. Comparison of three locomotion modes

Modes	DOFs	Working motors	Mobile Directions
Rolling	3	8	Two
Tumbling	4	4	One
Quadruped	8	12	Omnidirectional

IV. SWITCHING FUNCTION

In this section, we discuss the switching functions between the three locomotion modes. Based on the locomotion gaits, Figure 24 shows the relations of the locomotion modes. The key steps are finding the right switching states of the motion mode, which can be easily obtained from Table 6 in Appendix B. Then, we can get a rapid way for changing the locomotion mode. This function is very useful for the robot working in complexed out-door environments. It can switch its locomotion modes and therefore adapt different road conditions. For example, rolling mode will have a faster speed on flat ground; tumbling mode can be used for climbing stairs; and quadruped mode will be more useful on rough ground.

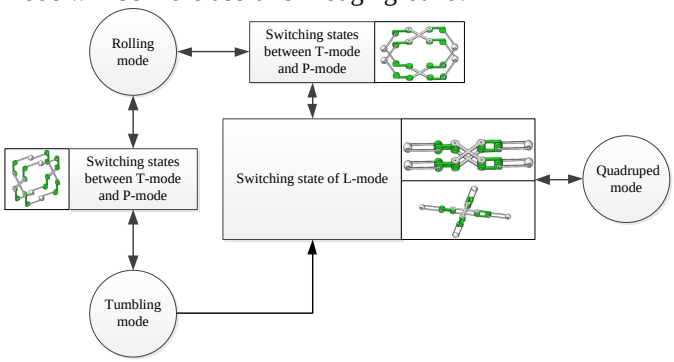

Fig. 24. The switching function of locomotion modes.

(1) Rolling and tumbling modes

As shown in Figure 25(b), this state is a typical switching state. If motors at A_i and E_i are working motors, the mechanism will have a tumbling mode (see Figure 25(c)); or if motors at B_i and D_i are working motors, it will have a rolling mode (see Figure 25(a)). Thus, the two modes can be directly switched at this state.

(2) Rolling and quadruped modes

When one platform is on the ground (see Figure 26(a)), the mechanism can deform into a switching state of L-mode (see Figure 26(b)). Then, we get the quadruped modes (see Figure 26(c)) by folding the arms at B_i. It can be seen that the two modes can be directly switched at the state in Figure 26(b).

(3) Tumbling and quadruped modes

Since the arms are always on the ground during a tumbling mode, tumbling and quadruped mode cannot be switched in a single state. As shown in Figure 27, there are three steps:

1) Making the platform on the ground using T-motion (see Figure 27(a-c));

2) Deforming into a switching state of L-mode (see Figure 27(c-e));

3) Expanding the legs (see Figure 27(f)).

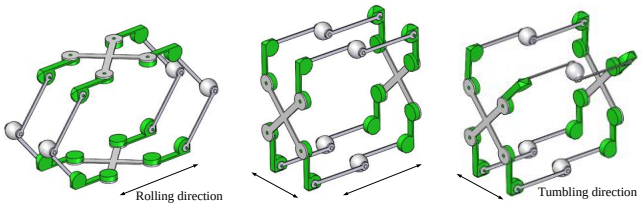

(a) (b) (c)

Fig. 25. Rolling mode and tumbling mode: (a) a rolling state, (b) a switching state, (c) a tumbling state.

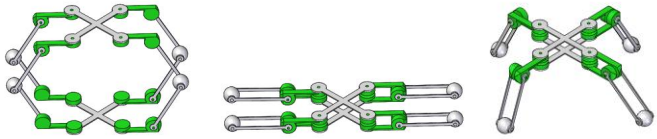

(a) (b) (c)

Fig. 26. Rolling mode and quadruped mode: (a) a rolling state, (b) a switching state of L-mode, (c) a quadruped state.

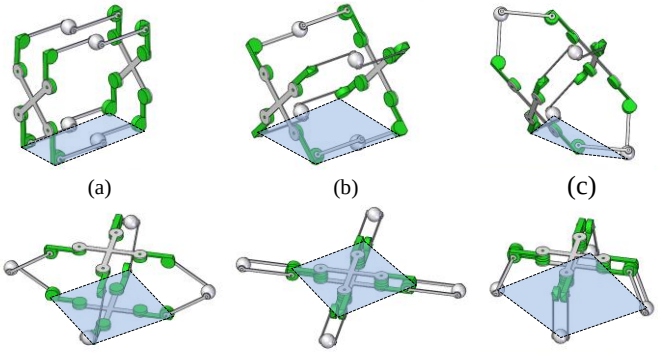

(a) (b) (c)

(d) (e) (f)

Fig. 27. Tumbling mode and quadruped mode.

V. PROTOTYPE AND EXPERIMENTS

The major purpose of this section is to verify the three locomotion modes of the robot with a real prototype at its corresponding states. Since it's very hard to control so many singularity positions at the same time, we switched these states manually in the next experiments. Figure 28 shows the prototype of our robot, and 12 motors are also marked on the figure. The parameters of the robot are given in Table 10.

Firstly, as shown in Figure 29, we use the relations of 12 motors in Tables 2, 3, and 5 to get the three typical sates of the mechanism. Then, based on T-mode, the robot can be folded into different small configurations, while the folding function allows the robot to be packed and transported conveniently. Figure 30(a) shows the folding operations using T-mode, and the total size of the robot is 850 mm ×850 mm ×80 mm. Figure 30(b) is the folding operations using the legs, and the size is 450 mm × 450 mm × 100 mm. Figure 30(c) is another folding operation using the legs, and the size is 250 mm ×250 mm ×80 mm.

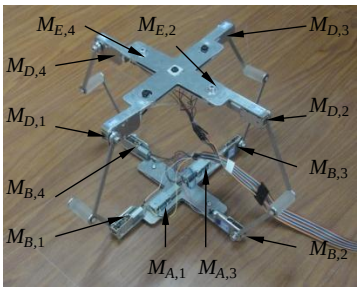

Fig. 28. The prototype of the parallel mechanism.

Table 10. Parameters of the prototype.

Total weight	3.5 kg
Total size	Max: 450 mm ×450 mm ×550 mm Min: 250 mm ×250 mm ×100 mm
DC motor	24V, 360 deg / s
The sizes of an arm	l_1 = 85 mm, l_2 = 20 mm l_3 = 100 mm, l_4 = 200 mm

Fig. 29. The motion modes of the upper platform (T-mode, P-mode, and L-mode).

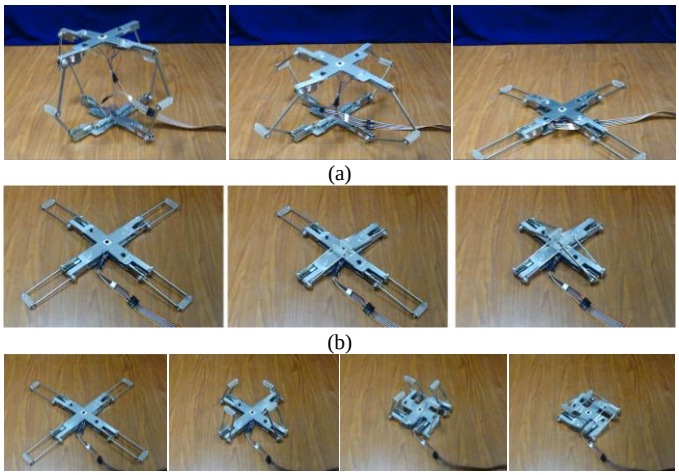

(a) (b) (c)

Fig. 30. Experiments of folding function.

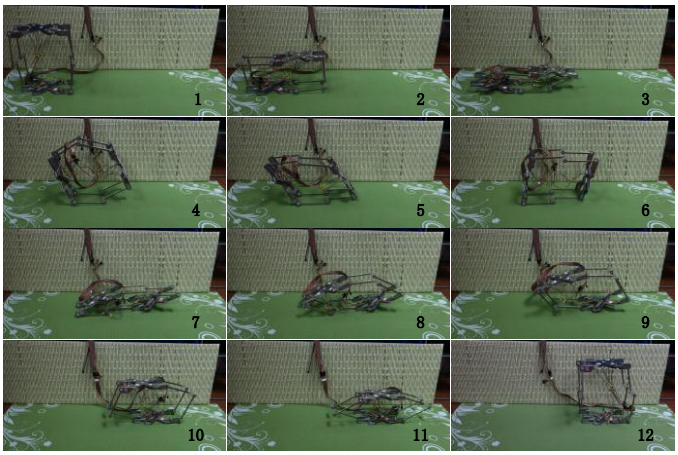

Fig. 31. Experiment of rolling locomotion.

Using the method in section 3, Fig, 31 shows the rolling experiment of the robot. Figure 32 is the experiments of tumbling mode. Figure 33 is the walking experiments based on the approach of static walk. These results verified the locomotion modes of the robots we have analyzed in Section 4.

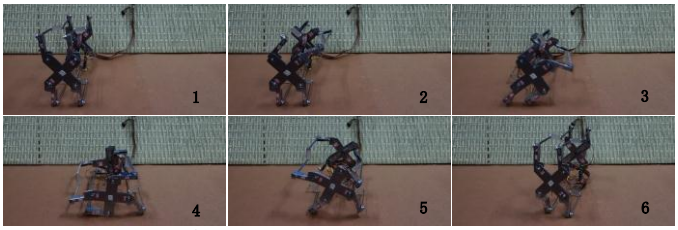

Fig. 32. Experiment of tumbling locomotion.

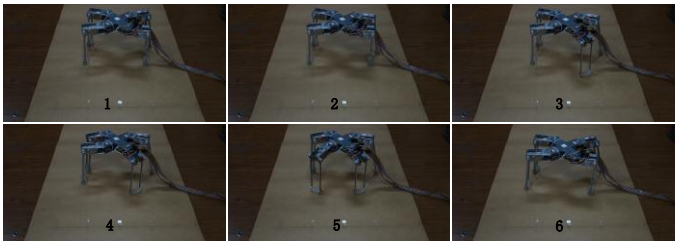

Fig. 33. Experiment of quadruped locomotion.

During the walking process, our robot can turn an arbitrary angle of φ by first lifting a pair of diagonal feet (e.g., C_1 and C_3) and then rotating the combined platforms by an angle of φ. Figure 34 shows the critical steps of a turning process. The positions of the motors are the same as the one shown in Figure 28, therefore we omit the marking of the motors in Figure 34 for clarity. Figure 24(f) shows the angle between the current state of the robot and its original state (the light shaded robot). In Figure 24, the axes of the working R joints are shown in red dashed lines, and the rotation direction is indicated by yellow arrows. The states of the robot in each figure of Figure 34 are as follows:

(a) Starting from the initial configuration, in which C_1 and C_3 are about to be lifted up.

(b) The hips of the first and third legs are about to be rotated.

(c) C_1 and C_3 are rotated by an angle of φ, and are about to be lowered down to touch the ground.

(d) C_1 and C_3 touch the ground, and C_2 and C_4 are then to be lifted up.

(e) The hips of the second and fourth legs are about to be rotated, C_2 and C_4 are about to be lowered down to the ground.

(f) The hips of the first and third legs are rotated by an angle of φ, C_2 and C_4 are touching ground. Compared with its original state (shown in light shaded) the body of robot has rotated by an angle of φ.

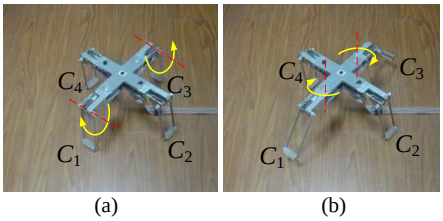

(a) (b)

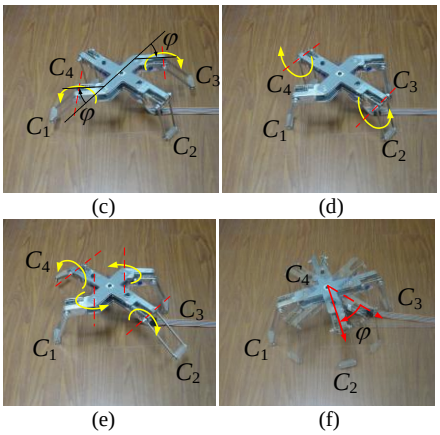

Fig. 34. Turning an angle of φ.

VI. Discussion and Conclusion

A. Discussion

In this section, we discuss the challenges and improvements of our robot. We have obtained and performed the three locomotion modes at their own modes in section III and IV. It's very important to realize the switching functions automatically. So, one of the biggest challenge is how to control the robot exactly reach such a plenty of singularity positions in the same times. The motors need to be actuated carefully at these positions. During our folding experiments, we found that if the upper platform is near enough to its singularity positions, it can be changed its mode from T-mode to L-mode. We shall use some soft materials and flexible links to design the mechanical body to reduce the requirements, and it is possible to use the fault-tolerance control method to realize our functions.

Both rolling and tumbling modes will cause some impacts when the robot moves on the ground. We can do the following things to reduce the impacts and improve its ability. (1) Optimize the gaits to make the robot roll or tumble at its lowest position. (2) Add soft elements or springs at the contact positions to absorb the impacts.

B. Conclusion

We put forward the idea of deforming the geometry and topology of a parallel mechanism such that it can operate either as a rolling mechanism or walking mechanism, with locomotion modes that are different than those of the original parallel mechanism. In particular, we present a reconfigurable mobile robot based on a four-arm parallel mechanism. The robot can be folded into three compact forms. Also our robot has three locomotion modes: tumbling, rolling, and walking with four legs. Using our prototype, the folding function was verified; in addition, a series of experiments were performed for each locomotion mode, i.e., tumbling, rolling, and four-leg walking. We comment that the robot can switch among these locomotion modes and therefore it can accommodate itself in different road conditions. The experiments proved the functionality of our design.

In future work, a new prototype will be carried out by two steps: (1) Using reconfigurable methods, to realize each locomotion mode, and switch manually at the first step. The gaits will be further studied and performed on a real prototype. (2) Combined those locomotion modes in a single system and performed automatically. We also plan to use the robot to carry a camera, a probe, or a mechanical arm to perform potentially hazardous tasks.

Acknowledgment

This work has been supported by National Natural Science Foundation of China (51175030), and the Natural Sciences and Engineering Research Council of Canada (NSERC). The authors gratefully acknowledge the financial support from Canada Research Chairs program.

References

[1] M. H. Raibert, "Legged robots," *Commun. ACM*, vol. 29, no. 6, pp. 499-514, Jun. 1986.

[2] J. A. T. Machado, and M. F. Silva, "An overview of legged robots," *in Proceedings of the MME International Symposium on Mathematical Methods in Engineering*, Ankara, Apr., 2006.

[3] L. Bruzzone and G. Quaglia, "Review article: locomotion systems for ground mobile robots in unstructured environments," *Mech. Sci.*, vol. 3, pp. 49–62, 2012.

[4] C. Grand, F. Banamar, F. Plumet and P. Bidaud, "Stability and traction optimization of a reconfigurable wheel-legged robot," *Int. J. Robot. Res.*, vol. 23, no. 10-11, pp. 1041–1058, 2004.

[5] D. P. Lu, E. B. Dong, C. H. Liu, Z. R. Wang, X. G. Zhang, M. Xu, and J. Yang, "Mechanical system and stable gait transformation of a leg-wheel hybrid transformable robot," in *Proc. IEEE/ASME Int. Conf. Adv. Intell. Mechatron.*, WG. Australia, Jul. 2013, pp. 530-535.

[6] S. Nakajima, "RT-Mover: A rough terrain mobile robot with a simple leg–wheel hybrid mechanism," *Int. J. Robot. Res.*, vol. 30, no. 13, pp. 1609–1626, 2011.

[7] S. Hirose and H. Takeuchi, "Study on roller-walker (basic characteristics and its control)," in *Proc. IEEE Int. Conf. Robot. Autom.*, Mpls. USA., Apr. 1996, pp. 3265–3270.

[8] T. Okada, W. T. Botelho and T. Shimizu, "Motion analysis with experimental verification of the hybrid robot PEOPLER-II for reversible switch between walk and roll on demand," *Int. J. Robot. Res.*, vol. 29, no. 9, pp. 1199–1221, 2010.

[9] S. J. Ylönen and A. J. Halme, "WorkPartner–Centaur like service Robot". in *Proc. IEEE/RSJ Int. Conf. Intell. Robots Syst.*, Lausanne, Switzerland, Oct. 2002, pp. 727–732.

[10] J. A. Smith, I. Sharf, and M. Trentini, "PAW: a hybrid wheeled-leg robot," in *Proc. IEEE Int. Conf. Robot. Autom.*, Orlando, USA, May. 2006, pp. 4043-4048.

[11] S. Yokota, H. Kobayashi and K. Kawabata, "Development of mobile system using leg-type crawler for rough terrain," *Ind. Robot: An International Journal*, vol. 31, no. 2, pp.218-223, 2004.

[12] F. Michaud, D. Létourneau, M. Arsenault, Y. Bergeron, R. Cadrin, F. Gagnon, M. Legault, M. Millette, J.-F. Paré, M.-C. Tremblay, P. Lepage, Y. Morin, J. Bisson, S., Caron, "AZIMUT, a leg-track-wheeled robot," in *Proc. IEEE/RSJ Int. Conf. Intell. Robots Syst.*, L.V. USA, Oct. 2003, pp. 2553–2558.

[13] M. Yim, K. Roufas, D. Duff, Y. Zhang, C. Eldershaw, and S. Homans, "Modular reconfigurable robots in space applications," *Auton. Robot.*, vol. 14, no. 2-3, pp. 225-237, 2003.

[14] E. Yoshida, S. Matura, A. Kamimura, K. Tomita, H. Kurokawa, and S. Kokaji, "A self-reconfigurable modular robot: Reconfiguration planning and experiments," *Int. J. Robot. Res.*, vol. 21, no. 10-11, pp. 903–915, 2002.

[15] W. M. Shen, M. Krivokon, H. Chiu, J. Everist, M. Rubenstein, and J. Venkatesh, "Multimode locomotion via SuperBot reconfigurable robots," *Auton. Robot.*, vol. 20, no. 2, pp. 165–177, 2002.

[16] A. Sproewitz, R. Moeckel, J. Maye, and A. J. Ijspeert, "Learning to move in modular robots using central pattern generators and online optimization," *Int. J. Robot. Res.*, vol. 27, no. 3-4, pp. 423–443, 2008.

[17] Y. Sugiyama and S. Hirai, "Crawling and jumping by a deformable robot," *Int. J. Robot. Res.*, vol. 25, no. 5-6, pp. 603–620, 2006.

[18] C. Paul, F. J. V. Cuevas, and H. Lipson, "Design and control of tensegrity robots for locomotion," *IEEE Trans. Robot.*, vol. 22, no. 5, pp. 944–957, 2006.

[19] S. C. Chen, K. J. Huang, W. H. Chen, S. Y. Shen, C. H. Li, and P. C. Lin, "Quattroped: a leg–wheel transformable robot," *IEEE/ASME Trans. Mechatronics*, pp. 1-10, 2013.

[20] C. C. Phipps, B. E. Shores, and M. A. Minor, "Design and quasi-static locomotion analysis of the rolling disk biped hybrid robot," *IEEE Trans. Robot.*, vol. 24, no. 6, pp. 1302-1314, Dec. 2008.

[21] C. C. Phipps and M. A. Minor, "Introducing the hex-a-ball, a hybrid locomotion terrain adaptive walking and rolling robot," in *Proc. 8th Int. Conf. Climb. Walk. Robots*, London, U.K., 2005, pp. 525–532.

[22] Y. Ota, Y. Inagaki, K. Yoneda, and S. Hirose, "Research on a six-legged walking robot with parallel mechanism," in *Proc. IEEE/RSJ Int. Conf. Intell. Robots Syst.*, Victoria, B.C., Canada, Oct. 1998, pp. 241–248.

[23] K. Yoneda, F. Ito, Y. Ota, and S. Hirose, "Steep slope locomotion and manipulation mechanism with minimum degrees of freedom," in *IEEE/RSJ Int. Conf. Intell. Rob. Syst.*, Kyongju, Korea, Oct. 1999, pp. 1897–1901.

[24] Y. Ota, K. Yoneda, F. Ito, S. Hirose, and Y. Inagaki, "Design and control of 6-DOF mechanism for twin-frame mobile robot," *Auton. Robot.*, vol. 10, no. 3, pp. 297-316, 2001.

[25] Y. Sugahara, T. Endo, H. Lim, and A. Takanishi, "Design of a battery-powered multi-purpose bipedal locomotor with parallel mechanism," in *Proc. IEEE/RSJ Int. Conf. Intell. Robots Syst.*, Lausanne, Switzerland, Oct. 2002, pp. 2658–2663.

[26] Y. Sugahara, T. Endo, H. Lim, and A. Takanishi, "Control and experiments of a multi-purpose bipedal locomotor with parallel mechanism," in *Proc. IEEE Int. Conf. Robot. Autom.*, Taipei, China, Sep. 2003, pp. 4342-4347.

[27] C. Liu, Y. A. Yao, "Biped RCCR mechanism," *ASME J. Mech. Design*., vol. 131, no. 3, pp. 031010.1–031010.6, 2009.

[28] C. Liu, H. H. Yang, Y. A, Yao, "A family of biped mechanisms with two revolute and two cylindric joints," *ASME J. Mech. Robot.*, vol, 4, no. 4, pp. 045002-1–045002-13, 2012.

[29] Z. Y. Qi, H. B., Wang, Z. Huang, and L. L. Zhang, "Kinematics of a quadruped/biped reconfigurable walking robot with parallel leg mechanisms," in *Proc. ASME/IFTOMM Int. conf. ReMAR 2009*, Jun. 2009, pp. 558–64.

[30] C. H. Liu, R. M. Li and Y. A. Yao, "An omnidirectional rolling 8U parallel mechanism," *ASME J. Mech. Robot.*, vol, 4, no. 3, pp. 034501-1-034501-06, 2012.

[31] Y. B. Tian and Y. A. Yao, "Constructing rolling mechanisms based on tetrahedron units," in *Proc. Int. Conf. ReMAR 2012*, Tianjing, China, Jul. 2012, pp. 221-232.

[32] Y. B. Tian and Y. A. Yao, "Dynamic rolling analysis of triangular-bipyramid robot," *Robotica*, vol. 33, no. 4, pp. 884-897, 2015.

[33] T. Yamawaki, O. Mori, and T. Omata, "Nonholonomic dynamic rolling control of reconfigurable 5 R closed kinematic chain robot with passive joints," in *Proc. IEEE Int. Conf. Robot. Autom.*, Taipei, China,, Sep. 2003, pp. 4054–4059.

[34] R. Aracil, R. Saltaren, and J. M. Sabater, "TREPA: Parallel climbing robot for maintenance of palm trees and large structures," in *Proc. 2th Int. Conf. CLAWAR*, London, UK, 14–15 Sep. 1999, pp. 453–461.

[35] R. Aracil, R. Saltarén, and O. Reinoso, "Parallel robots for autonomous climbing along tubular structures," *Robot. Auton. Syst.*, vol. 42, no. 2, pp. 125–134, 2003.

[36] A. Bekhit, A. Dehghani, and R. Richardson, "Kinematic analysis and locomotion strategy of a pipe inspection robot concept for operation in active pipelines," *Int. J. Mech. Eng. Mechatronics*, vol. 1, no. 1, pp. 15–27, 2012.

[37] X. W. Kong, C. M. Gosselin, and P. L. Richard, "Type synthesis of parallel robots with multiple operation modes," *ASME J. Mech. Design*., vol. 129, no. 6, pp. 595–601, 2007.

[38] X. W. Kong, "Reconfiguration analysis of a 3-DOF parallel mechanism using Euler parameter quaternions and algebraic geometry method," *Mech. Mach. Theor.*, vol. **74**, pp. 188–201, 2014.

[39] Z.H. Miao, Y. A. Yao, and X. W. Kong, "Biped walking robot based on a 2-UPU+2-UU parallel mechanism," *Chin. J. Mech. Eng-E.*, vol. 7, no. 2, pp. 269–278, 2014.

[40] Y. B. Tian, Y. A. Yao,, W. Ding, and Z. Y. Xun, "Design and locomotion analysis of a novel deformable mobile robot with worm-like, self-crossing and rolling motion," *Robotica*, DOI: 10.1017/S0263574714002689, 2015.

[41] Y. B. Tian, X. Z. Wei, A. Joneja, and Y. A. Yao, Sliding-crawling parallelogram mechanism. *Mech. Mach. Theor.*, vol. 78, pp. 201-228, 2014.

[42] Y. B. Tian, Y. A. Yao, and J. Y. Wang, "A rolling 8-bar linkage mechanism," *ASME, J. Mech. Robot.*, vol. 7, no. 4, pp. 041002, 2015.

[43] C. M. Gosselin and J. Angeles, "Singularity analysis of closed-loop kinematic chains," *IEEE T. Robotic. Autom.*, vol. 6, no.3, pp. 281-290, 1990.

[44] J. S. Dai and J. R. Jones, "Mobility in metamorphic mechanisms of foldable/erectable kinds," *ASME J. Mech. Design.*, vol. 121, no. 3, pp. 375–382, 1999.

[45] J. S. Dai, D. L. Li, Q. X. Zhang and G. G. Jin, "Mobility analysis of a complex structured ball based on mechanism decomposition and equivalent screw system analysis," *Mech. Mach. Theor.*, vol. 39, no. 4, pp. 445–458, 2004.

[46] J. Sastra, S. Chitta, and M. Yim, "Dynamic rolling for a modular loop robot," *Int. J. Robot. Res.*, vol. 28, no. 6, pp. 758-773, 2009.

[47] C. H. Liu, Y. A. Yao, R. M. Li, Y. B. Tian, N. Zhang, Y. Y. Ji, and F. Z. Kong, "Rolling 4R linkages," *Mech. Mach. Theory*., vol. 48, pp. 1–14, 2012.

[48] C. Theeravithayangkura, T. Takubo, K. Ohara, Y. Mae, and T. Arai, "Dynamic rolling-walk motion by the limb mechanism robot ASTERISK," *Adv. Robotics*, vol. 25, pp. 75-91, 2011.

[49] *Springer.Handbook of Robotics*, B. Siciliano and O. Khatib, Springer-Verlag, New York, USA, 2008, pp. 378–383.

[50] S. Hirose, Y. Fukuda, K. Yoneda, A. Nagakubo, H. Tsukagoshi, K. Arikawa, G. Endo, T. Doi, and R. Hodoshima, "Quadruped walking robots at Tokyo Institute of Technology," *IEEE Robot. Autom. Mag.*, vol, 16, pp. 104-114, 2009.

Appendix

Table 6. The motion modes and switching states of the mechanism.

Type	Conditions	States	Motion
T-mode	$R_{Ai} = R_{Ei}$, (for i = 1, 2, 3, 4) $R_{Bi} \neq R_{Di}$, (for i = 1, 2, 3, 4)	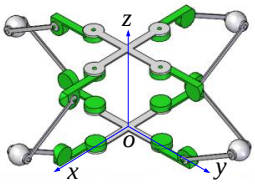	One translational motion along oz-axis
P-mode	$R_{Bi} // R_{Bj}$ $R_{Bi} \neq R_{Bj}$, (for i and j = 1, 2, 3, 4)	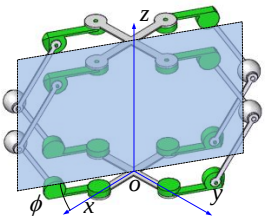	Planar motion in the p plane (the plane p has an angle of ϕ with respect to xoz plane, and $\phi \in$ [0 180] deg)
	$R_{B1} = R_{B4}$, $R_{B2} = R_{B3}$ $R_{B1} // R_{B2}$; or $R_{B1} = R_{B2}$, $R_{B3} = R_{B4}$ $R_{B1} // R_{B3}$;	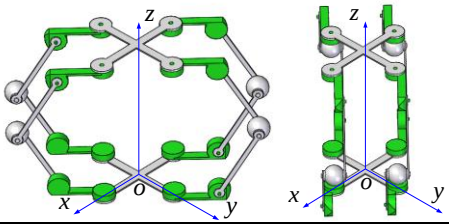	Planar motion in the plane with ϕ = 45 *deg*, or ϕ = –45 *deg*
	$R_{B2} = R_{B4}$ or $R_{B1} = R_{B3}$ $R_{Bi} // R_{Bj}$ (for i and j = 1, 2, 3, 4)	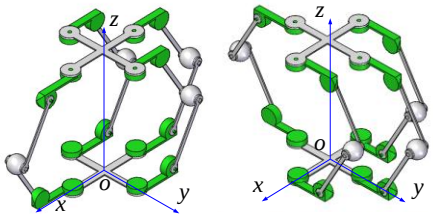	Planar motion in the xoz plane or yoz plane
R-mode	$R_{B1} = R_{B4} = R_{D1} = R_{D4}$ $R_{B2} = R_{B3}$, $R_{B1} // R_{B2}$ or $R_{B2} = R_{B3} = R_{D2} = R_{D3}$ $R_{B1} = R_{B4}$, $R_{B1} // R_{B2}$	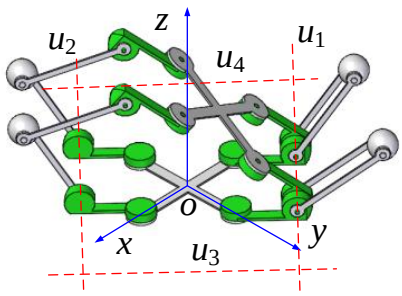	Rotational motion about line $u_1$or u_2
	$R_{B1} = R_{B2} = R_{D1} = R_{D2}$ $R_{B3} = R_{B4}$, $R_{B1} // R_{B3}$ or $R_{B3} = R_{B4} = R_{D3} = R_{D4}$ $R_{B1} // R_{B3}$, $R_{B1} = R_{B2}$		Rotational motion about line u_3 or u_4
L-mode	$R_{Ai} = R_{Ei}$, $R_{Bi} = R_{Di}$ (for i = 1, 2, 3, 4)	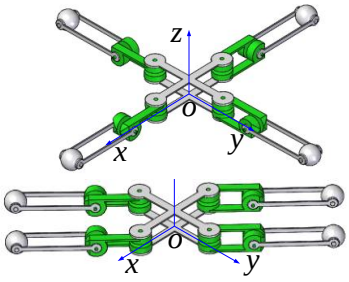	No motion